Precursory predictors of the onset of stick-slip frictional instability

Lu Gu [a], Shengwang Hao [a,*], Derek Elsworth [b]

[a] *School of Civil Engineering and Mechanics, Yanshan University, Qinhuangdao, China*
[b] *Energy and Mineral Engineering, Geosciences, G3 Center, and EMS Energy Institute, Pennsylvania State University, University Park, PA, USA*

ABSTRACT

Defining precursory phenomena that forewarn the onset of stick slip events remains an elusive but central goal in earthquake and other failure forecasting. We present a method to define the timing of instability by separately decoupling velocity and inertial effects in a spring-slider system. System state is defined in phase-space by velocity and inertia that in turn control critical stiffness and define the onset of instability while sliding velocity $V = V_L k/(k + dF/du)$ remains finite. A general energy analysis defines velocity and inertial effects (coefficients) that act against each other to promote/suppress instability by respectively increasing/decreasing critical stiffness. Repetitive stick-slip experiments define features of stick-slip cycles and identify a precursory trend in accelerating slip that precedes the onset of unstable sliding. We represent this precursory acceleration (dV/dt) immediately preceding instability by a general power-law relation $dV/dt = AV^{\alpha}$ that reduces to $V = B(c_i + t_i\text{-}t)^{-\beta}$. This represents the "true" timing of the onset of stick slip, t_i relative to that "projected" from the linearization of the precursory data, t_f, with $t_f = c_i + t_i$. c_i represents the small offset between the "predicted" and "true" timing of the onset of stick slip resulting from velocity and inertial effects and may be considered as the error in prediction. This error is one-order of magnitude smaller (~3 ms) than the lead-time that forewarns of the event (~40 ms) in our experiments and thus is useful as a predictor. Three independent methods using power-law, linear and criticality relationships confirm the fidelity of the timing of the slip instability transition evident in the stick slip data. This theoretical treatment suggests that the underlying physical meaning of the parameter c in the modified Omori law $R \sim (c + t_M\text{-}t)^{-q}$ is the time of the main shock in advance of the timing of the singularity predicted for an ideal response.

1. Introduction

Stick-slip instabilities (Rabinowicz, 1956; Brace & Byerlee, 1966; Shimamoto et al., 1980; Baumberger et al., 1994; Cui et al., 2017) are a characteristic feature of earthquake nucleation and as such are important in understanding mechanisms of material failure in general (Gnecco, 2018; Xing & Han, 2020; Lin et al, 2020; Fávero Neto et al., 2020; Kasyap et al., 2021) and natural earthquakes (Brace & Byerlee, 1966; Scholz, 1998) in particular. Such frictional phenomena are also common in engineering systems over a wide range of length-scales (nanostructures to engineered systems) (Rabinowicz, 1956; Urbakh et al., 2004; Bhushan, B. 2013). Describing trends in sliding in the approach to the slip instability transition is undoubtedly significant in understanding sliding behaviors and in exploring methods to predict imminent instability – viz. earthquakes and other catastrophic rupture.

Earthquakes result from instability of a natural fault under far-field loading in elastic crust where the surrounding elastic rock mass accu-

mulating strain until the fault slips – and the stored strain energy is rapidly ejected. Frictional instability is often explored by examining contacting surfaces or gouge in relative motion – such as in direct-shear – and represented by a spring-slider system (Fig. 1). The slider in Fig. 1 represents frictional resistance between two surfaces and the spring represents the elastic behaviour of the surrounding rock and the accumulation of stress that will eventually overcome that resistance. Sliding is driven by a driving force, *F* that extends the spring at a constant rate. *Static* analysis predicts that the frictional slip instability occurs when the tangent to the slope (dF/du) of force-versus-sliding-displacement curve is equal to the (negative) system stiffness, where *u* represents the sliding displacement. For a *dynamic* system, both analytical (Rice and Ruina, 1983; Gu et al., 1984; Rice and Tse, 1986; Gu and Wong, 1991; Im et al., 2017; 2019) and numerical results (Im et al., 2019) based on rate and state laws (Dieterich, 1979; Ruina, 1983) show that two distinct dynamic regimes exit. These regimes are defined as "stick–slip" in the quasi–static (slowly loaded) regime and as "quasi–harmonic
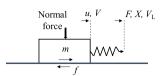
Fig. 1. Single degree of freedom elastic spring-slider system.

oscillations" in the dynamic (rapidly loaded) regime. These regimes are defined by the dynamic frictional instability coefficient (Im et al., 2019)

$$\eta = \frac{MV^2}{\sigma a D_c} \tag{1}$$

that highlights the effects of mass and velocity (V) on the slip instability transition. In this, M is mass per unit area (kg/m^2), σ is normal stress, D_c is a critical slip distance that characterizes the evolution of friction following a perturbation and a is a nondimensional parameter that defines the magnitude of the direct velocity-dependent effect in the rate and state friction law. But rate and state laws are phenomenological models and most 'state variables' cannot yet be quantitatively related to physical system properties (Urbakh et al., 2004; Ruina, 1983; Carlson and Batista, 1996). Here, we demonstrate the effects of mass and velocity on the slip instability transition using detailed experimental measurements and a detailed analysis of velocity and inertial effects.

In this paper, we present a theoretical explanation of slip instability transition based on energy equilibrium, rather than rate and state laws, and decouple velocity and inertial effects. We report detailed measurements of shear displacement on interfaces in granite showing typical stages of stick-slip events. Specifically, we: 1) Characterize impacts of both load point velocity and inertia on the evolving slip instability and provide order-of-magnitude evaluations of these two effects; 2) Identify robust precursors to the onset of stick-slip from detailed but generic laboratory observations; and 3) Define relationships linking the dynamic slip instability transition to an idealized singularity to use in forewarning of the nucleation of stick-slips.

2. Theoretical analysis of frictional slip instability

2.1. Slip instability criterion

We analyze frictional instability as a one-dimensional spring-slider system (Fig. 1) loaded by a constant velocity load point. Here, the slip instability is controlled by loading conditions and frictional behavior. Following peak force, that is the maximum force in each stick-slip cycle, a change in the load-point force (dF) resulting from an increment of the load point displacement (dX) induces a sliding increment of du, and involves a recovery in deformation (RID) of the elastic spring as du_e = -dF/k. Here, k represents the stiffness of the elastic spring, F is the external force and the sign of dF is negative after peak force corresponding to a reduction with increasing displacement.

The change in work dW is given by the product of the mean force as it changes from F to F + dF (i.e., F+(dF/2)) and the distance du moved while it is applied, or [F+(dF/2)]du. A stability analysis of sliding depends on the interplay between three energetic quantities: the increment of work dW=(F + dF/2)dX done by the external load, the release of energy dW_e=(F + dF/2)du_e from the elastic spring as it contracts and the work dW_b=(F + dF/2)du required to displace the slider by an increment du. The work dW_b generally comprises two components, *viz.* the work consumed by the frictional force and the change in kinetic energy of the slider.

The system is out-of-equilibrium and unstable if

$$dW_b < dW + dW_e \tag{2}$$

or

$$du < dX + du_e. \tag{3}$$

Physically, these two equations state that the instability is defined such that the available energy is larger than the work required to promote sliding, or that the sliding response du cannot keep-up with the total imposed displacement defined as the combination of dX and du_e.

Differentiation of equation (3) with respect to time defines that instability occurs when

$$1 < \frac{V_L}{V} - \frac{1}{k}\frac{dF}{du} \tag{4}$$

where V_L = dX/dt is the velocity of the load point, and V = du/dt is the sliding velocity of the slider. For static loading, V_L = 0, and the critical condition for the slip transition from stability to instability is

$$\frac{dF}{du} = -k \tag{5}$$

and the critical stiffness k_c = -dF/du. Otherwise, the critical condition for the instability transition becomes

$$1 - \frac{V_L}{V} = -\frac{1}{k}\frac{dF}{du} \tag{6}$$

i.e. the tangential slope dF/du of the force (F) to the sliding displacement (u) is equal to $-k(1 - V_L/V)$.

2.2. Velocity and inertial effects

Note that the load-point force F is the sum of both frictional resistance f and inertial component $m\dot{V}$, i.e.

$$F = f + m\dot{V} \tag{7}$$

Where m is the mass of the slider, and

$$\frac{dF}{du} = \frac{df}{du} + m\frac{d\dot{V}}{du} \tag{8}$$

Combining equations (6) and (8) gives

$$\frac{df}{du} + m\frac{d\dot{V}}{du} = -k\left(1 - \frac{V_L}{V}\right) \tag{9}$$

This can be rewritten in a non-dimensional form as

$$1 - \chi = \lambda(1 - \zeta) \tag{10}$$

And sliding is stable when

$$1 - \chi < \lambda(1 - \zeta) \tag{11}$$

where

$$\lambda = k/k_{esl} \tag{12}$$

representing the ratio of spring stiffness with respect to the equivalent stiffness k_{esl} of the slider's resistance with

$$k_{esl} = -df/du. \tag{13}$$

Post peak force, df/du becomes negative so that λ is positive.

We define "load velocity effect coefficient" ζ and "inertial effect coefficient" χ as

$$\zeta = V_L/V \tag{14}$$

and

$$\chi = -m\frac{d\dot{V}/du}{df/du} \tag{15}$$

According to equation (10), the critical stiffness k_{cd} of the spring for the dynamic instability can be expressed as

$$k_{cd} = k_{esl}(1 - \chi)/(1 - \zeta) \tag{16}$$

The dimensionless parameter ζ describes the effect of the velocities

V_L for the applied load and V of the slider: ζ tends to infinity when V_L dominates, and ζ tends to 0 when the slider moves much faster than the load point. After exceeding the peak force F, the elastic spring releases its stored energy as it restores its deformation. As a consequence, the sliding velocity of the slider is faster than the load-point velocity, *i.e.* $V > V_L$ so that ζ decreases from 1 as force changes from its peak to the value at the slip instability transition.

Eqn. (16) shows that load-point velocity plays a key role in the instability transition to frictional sliding. The effect of V_L on k_{cd} is negligible when V_L is very small, but becomes significant when V_L is large so that the ratio of V_L/V is large. Under this condition, the velocity effect ζ becomes significant and cannot be neglected in determining the transition to instability.

The dimensionless parameter χ represents the ratio of the rates of change of inertial force to frictional force, each normalized with respect to sliding displacement. The negative sign for Eqs. (13) and (15) indicate that the value of $\mathrm{d}f/\mathrm{d}u$ is negative after peak force prior to the slip instability transition point but $\mathrm{d}\ddot{u}/\mathrm{d}u > 0$ (see following section on experimental results). Thus, the sign of $\frac{\mathrm{d}\dot{V}/\mathrm{d}u}{\mathrm{d}f/\mathrm{d}u}$ is negative so that the value of χ must be positive. This parameter has the form of a surrogate "Reynolds Number for solids" and ranges from 0 (low inertia) to 1 (high inertia).

Rewriting Eqn. (15) by eliminating the common normalizing parameter of displacement yields

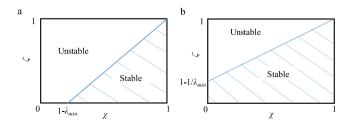$$\chi = -m\frac{\mathrm{d}\dot{V}}{\mathrm{d}f} \tag{17}$$

Thus χ represents the ratio of the change in inertial force to frictional force. When mass is fixed, the reciprocal of χ represents the rate of change of frictional resistance with respect to acceleration. χ is large when acceleration changes rapidly with respect to frictional resistance and must then be accommodated in any analysis of the instability transition.

Eqn. (10) gives that the critical value of $\mathrm{d}f/\mathrm{d}u$ at the point of instability such that

$$\left(-\frac{\mathrm{d}f}{\mathrm{d}u}\right)_{cd} = k(1-\zeta)/(1-\chi) \tag{18}$$

Post-peak force, the slope $\mathrm{d}f/\mathrm{d}u$ of the frictional force (f) versus the sliding displacement (u) becomes negative and values of $(-\mathrm{d}f/\mathrm{d}u)$ increase towards a maximum. When the elastic stiffness k is fixed, Eqn. (18) indicates that the "load velocity coefficient" ζ predicts that unstable sliding will occur earlier because it decreases the critical value $(-\mathrm{d}f/\mathrm{d}u)_{cd}$ for the initiation of unstable sliding from $k/(1-\chi)$ to $k(1-\zeta)/(1-\chi)$.

Fig. 2 illustrates stable and unstable regimes of sliding behaviours in χ versus ζ phase space. It should be mentioned that the slip instability occurs in the phase ranging from the point of peak force to the point when (-df/du) reaches its maximum value where λ has its minimum value ($\lambda_{\min}$). Thus, we plot stable and unstable regimes according to two

Fig. 2. Stable and unstable regimes of sliding behaviours in a χ versus ζ phase plot when (a) $\lambda_{\min} \leq 1$; (b) $\lambda_{\min} \geq 1$. λ is the ratio of spring stiffness k with respect to the equivalent stiffness of the slider's resistance (-df/du). $\lambda_{\min}$ is the minimum value when (-df/du) reaches its maximum. The stable regime is shaded.

the cases when $\lambda_{\min} \leq 1$ or $\lambda_{\min} \leq 1$. Sliding is stable when the values of χ and ζ are located in the area under the critical boundary line.

2.3. Instability transition and singularity points

Equation (4) can be rewritten as $V < V_L k/(k + \mathrm{d}F/\mathrm{d}u)$ implying that the sliding velocity response cannot keep-up with the required velocity that is driven by the available work. The condition where $-\mathrm{d}F/\mathrm{d}u = k(1 - V_L/V)$ or $V = V_L k/(k + \mathrm{d}F/\mathrm{d}u)$ represents the critical point where unstable slip initiates. Post peak-force, $\mathrm{d}F/\mathrm{d}u$ decreases from zero, so that the slip instability transition occurs before it evolves to the condition $\mathrm{d}F/\mathrm{d}u = -k$.

From static analysis, at the transition to instability $\mathrm{d}F/\mathrm{d}u = -k$ the sliding velocity tends to infinity. Thus, the transition point where $\mathrm{d}F/\mathrm{d}u = -k$ is also a singularity. In a static analysis, the shear force F must equate to the frictional force f. In practice, the sliding velocity is finite but not so rapid that unstable slip always initiates before it reaches the point of singularity. The separate velocity (ζ) and inertial (χ) effects distinguish the timing of the onset of the dynamic slip instability from the timing of the (ideal) singularity point. Thus, the relative magnitudes of these two parameters control the difference in timing between the (real) dynamic slip instability and the (ideal) singularity.

The following experimental results confirm that the accelerating phase may indeed be divided into two stages separated by this instability transition point. Accelerated sliding in the earlier stage is a stable precursory acceleration process that is then followed by unstable slip – enabling a rational precursor to forewarn of the impending instability.
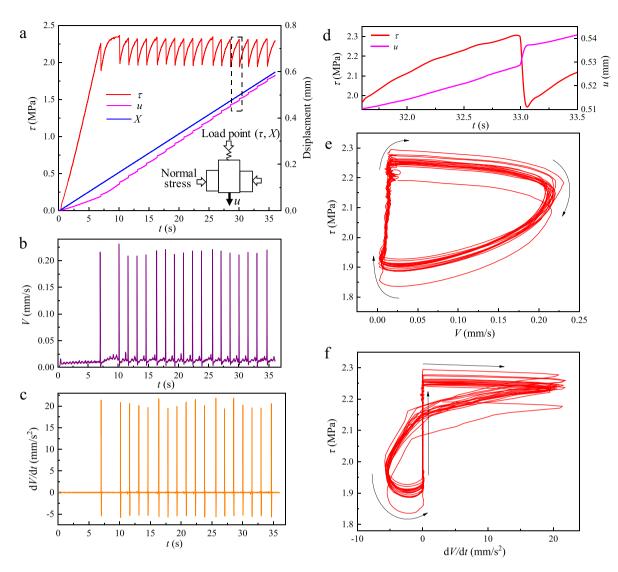
3. Typical stages transitioning from precursory acceleration through unstable slip to arrest

3.1. Experimental procedure and materials

Stick slip experiments are conducted in a biaxial loading apparatus under double direct shear configuration at room temperature (~20 °C) and humidity (~31 % relative humidity). All tests are performed in the Mechanics Laboratory of Yanshan University, China. Two fault zones delineate three prismatic blocks of granite (see inset in Fig. 3a) allowing shearing between the roughened surfaces. The nominal frictional contact area is 36 mm × 40 mm. Shear stresses are applied by the vertical ram of the Instron 5982 testing machine with normal stresses applied horizontally. Normal stresses are applied by a gas compression actuator set at a controlled constant gas pressure. The vertical load system with an elastic stiffness of ~ 144 kN/mm in the current experiments is analogous to the elastic spring in Fig. 1. Eqn. (10) indicate its significant effects on sliding behaviours and the transition from stable to unstable slip.

The granite sample comprises 46.5 % diopside, 19.5 % albite, 33.9 % anorthite and 0.2 % quartz based on X-ray diffraction (XRD) analysis. The mean crystal size of the rock is ~ 680 μm (Hao et al., 2017), the uniaxial compressive strength is ~ 222 MPa, and Young's modulus is ~ 38 GPa. We use granite as a typical host of crustal faults and representative of stick slip behavior common in other igneous and basement rocks. This is a common and typical analog for such behavior.

Sliding displacement in the experiments, *u,* is monitored by a linear variable differential transformer (LVDT) attached under the central sliding block. The load point displacement (X) combines the deformation of the loading apparatus and that of the sliding displacement (u). Shear force F, load point displacement and sliding displacement are recorded digitally and synchronously stored at a sampling rate of 1000 Hz. In calculations of velocities and accelerations based on differential calculations, we control the sampling rate in each incremental time step so that the data differences are larger than the fluctuations. It should be noted that the frictional resistance f on contacting surfaces is somewhat different from the shear force F and is difficult to directly measure in experiments. Fig. 3 defines shear stress as $\tau = F/A$, where A is the total

Fig. 3. Experimental data showing progress of a sequence of repetitive stick–slip events when the normal stress is 3.4 MPa. Shear stress $\tau = F/A$, where A is the total area of the contacting frictional surfaces. (a) Shear stress, τ, and sliding displacement, u, (b) sliding velocity, (c) acceleration during repetitive stick slip failures under monotonically increasing load point displacement, X. Insets (a): schematic of double-direct shear configuration. (d) Zoom-in on a single stick slip event. Phase diagram showing shear stress evolution against sliding (e) velocity and (f) acceleration during stick slip cycles.

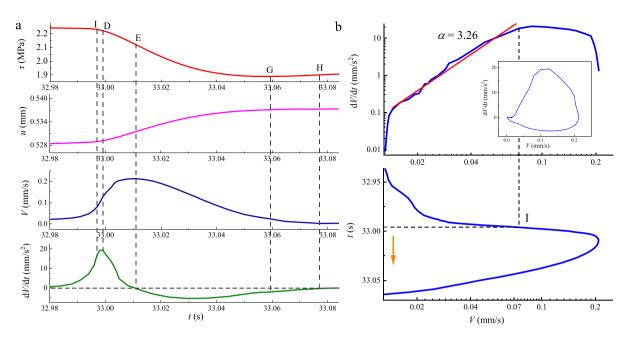area of the contacting frictional surfaces.

3.2. Typical stages

A typical sequence of repetitive stick-slips generated when the normal stress is 3.4 MPa and the loading velocity $V_L = 1$ mm/min is shown in Fig. 3. After the first two stick slip events the stick slip behavior becomes near-periodic. In each stick-slip cycle, a slip instability transition occurs (Fig. 3d) post peak force. Sliding velocity and acceleration are shown continuously in Fig. 3b and 3c for the full experimental sequence and indicate that maximum velocities and accelerations for all stick-slip cycles are mono-periodic and highly repeatable.

Phase diagrams for shear force evolving with changes in sliding velocities V and accelerations $\dot{V}$ are shown in Fig. 3e and 3f to define repetitive and repeatable stick-slip cycles. During each "stick" period, the acceleration remains near-zero and the sliding velocity changes only very slowly. During this, the shear force increases linearly with sliding velocity.

In the unstable cycle the system transits from acceleration to deceleration with key points characterizing first the initiation of the instability transition (point I in Fig. 4), the maximum acceleration (point D in Fig. 4), the maximum velocity (point E in Fig. 4), the minimum acceleration (point L in Fig. 4) and then the minimum shear force (point G in Fig. 4). Consequently, evolution of sliding during individual stick-slip event shows several stages characterized by changes in velocity and acceleration (Fig. 4). The first stage is an acceleration characterized by monotonic increases in sliding accelerations until reaching the maximum value denoted by point D in Fig. 4. During the next phase (D to E) the acceleration decreases until the velocity of sliding reaches its maximum. At the maximum velocity (point E) the acceleration is zero and the shear force is equal to the frictional force. This is followed by an "undershoot" in accelerations with decelerating sliding velocity characterized by negative acceleration until point H. Point G is where the shear force is a minimum and represents the end of the unstable slip cycle.

Following the unstable slip cycle, sliding and deceleration continue but the shear force, frictional force and the deformation of the system all increase. This stage is represented between points G and H in Fig. 4. This is characterized by lower sliding velocity than that during unstable sliding and represents a stage of intermediate adjustment, returning from acceleration "undershoot" to a quasi-static state. It is during this transition that sliding transits from unstable state to quasi-steady where

Fig. 4. Details of a single stick slip event (e.g. from Fig. 3d) illustrating typical stages. (a) Typical evolutions of shear stress, sliding displacement, velocity and acceleration. Ordinates represent - D: maximum acceleration, E: Maximum velocity, G: minimum shear stress, H: approaching rest state before next cycle. (b) Log-log curve of accelerations versus velocity showing Voight's relation well representing behavior in the proximity of the slip instability transition point I (above) and on the corresponding curve of velocity versus time (below). Inset: entire phase-space cycle of acceleration versus velocity. Red line in (b) shows a linear fitted line. The unstable acceleration process after point I clearly deviates from the linear trend. Phase IG: unstable process.

the sliding velocity reaches its minimum at point H. The sliding velocity V at point H is again equal to the loading velocity V_L, the shear force again equal to the frictional force and the system returns to a quasi-steady state - ready to begin the next stick-slip cycle.

4. Precursory acceleration approaching the slip instability transition - power law

An acceleration in the rate of change ($d\Omega/dt$) of some response quantity (Ω) (such as displacement or AE counts) may be used as a fundamental index of a system approaching instability point (Voight, 1988, 1989; Kilburn, 2003, 2012). This may be described by Voight's relation (Voight, 1988, 1989) as

$$d^2\Omega / d t^2 = A(d\Omega/d t)^\alpha \qquad (19)$$

where A and α are constants.

Fig. 4b illustrates the log–log relation between sliding acceleration and velocity representative of our data. The linear trend to the left (Fig. 4b) in the proximity of the instability transition indicates that this power law relationship adequately characterizes the dynamic slip instability, i.e.

$$\dot{V} = A \; V^\alpha \qquad (20)$$

However, beyond the slip instability transition (point I) a deviation from this linear trend is clearly apparent. This transition distinguishes the precursory accelerating sliding from the forthcoming unstable acceleration.

We examine the utility of this power law relationship (Eqn. (20)) as a *bona-fide* and robust precursory trend – that may be used to forewarn of the onset of stick slip. Fig. 5 shows the data for four other unstable slip events, confirming the ubiquity of this signature. Following low-sliding-velocity and accelerating stages, the distinct and repeatable power law form of the precursory acceleration in the sliding velocities in the proximity of the slip instability transition indicates that Voight's relation indeed also holds for the stick slip events.

From rearrangement of Voight's relation (equation (19)), we recover

the relation [Hao et al., 2016, 2017]

$$V/ \dot{V} = (\alpha - 1) \; (t_f - t) \qquad (21)$$

to describe the time to failure, where t_f represents the failure time where the ratio of rate to acceleration $V/ \dot{V}$ tends to zero, i.e. where acceleration tends to infinity. V and $\dot{V}$ represent velocity and acceleration, respectively. In stick slip cycles, neither acceleration nor velocity tend to infinity and the slip instability transition can be defined as the time when $V/ \dot{V}$ is a minimum. Experimental results (Fig. 6) confirm that this method indeed returns consistent results to define the timing of the slip instability transition. The approximately linear portion of the velocity-versus-acceleration relation in proximity to the instability transition point (Fig. 6) shows that this linear relation of Eqn. (21) faithfully represents the current experiments.

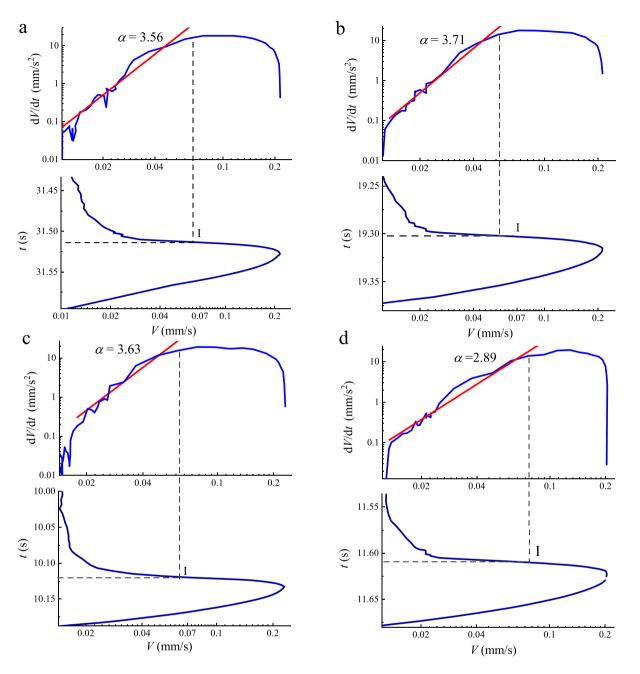The critical slip instability condition of Eqn. (6) may be defined as

$$- \; d F/d u = k \; (1 - V_L/V) \qquad (22)$$

at the point of slip instability. Fig. 6 shows zoomed-in data for four typical experiments for both $-dF/du$ and $k(1-V_L/V)$ over the transition time separating peak force from unstable sliding. The intersection between these two curves (where $-dF/du = k(1-V_L/V)$) following peak force identifies the instability transition point. After this transition to instability, the magnitude of $-dF/du$ decreases below that of $k(1-V_L/V)$, as suggested by Eqn. (4). The observation that (i) this instability transition may also be determined from Fig. 6 by using Eqn. (21) and that (ii) this conforms with the definition of criticality defined by Eqn. (22) confirms that the precursory power law indeed conforms to the Voight relation of Eqn. (20).

Based on Voight's relation, a power law relationship in the velocity V with respect to time to failure can be deduced (Voight, 1988, 1989; Voight and Cornelius, 1991; Kilburn and Voight, 1998; Main 1999; Kilburn, 2003, 2102; Bell et al., 2011; Hao et al., 2016, 2017) as

$$V = B \; (t_f - t)^{-\beta} \qquad (23)$$

where B is a constant and $\beta = 1/(\alpha-1)$ is the power law exponent.

Fig. 5. Four events selected to illustrate Voight's relation (red line) in fitting accelerations in the proximity of the slip instability transition. After an initial slow acceleration, the more rapid accelerations due to sliding are well described by Voight's relation. Red line: linear fitted line for the Voight relation with slope equal to the exponent α with values of 2.89 ~ 3.71. Following unstable acceleration the data clearly deviate from the trend of Voight's relation.

Equation (23) shows that the velocity becomes infinite at the time of failure t_f. The prior theoretical analysis indicates that the singularity does not necessarily coincide with the slip instability transition time. Thus, for the slip instability defined as Eqn. (6) for which the velocity is finite, we rewrite the power law acceleration of Eqn. (23) as

$$V = B \ \left(c_i + t_i - t \right)^{-\beta} \tag{24}$$

where $t_f = c_i + t_i$) where t_i is the timing of the actual onset of instability (e.g. point I in Fig. 4), and t_f is the projected timing of this onset recovered from the linearization. Thus parameter c_i is the small offset between projected and actual timing ($c_i = t_f - t_i$). In our experiments, the power law exponent for the precursory accelerations β is ~ 0.42 with $\alpha \approx 3.4$ (Figs. 4 and 5).

A similar power law relationship is represented by the modified Omori (or Omori-Utsu) law (Hainzl et al., 1999; Jones and Molnar, 1979, Utsu et al., 1995)
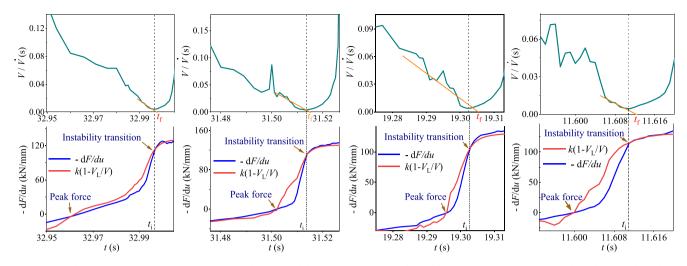
$$R \sim (c + t_M - t)^{-q} \tag{25}$$

and has been suggested to describe the occurrence rates R of precursory foreshocks before a main shock. Where t_M is the timing of the main shock and c is a small constant. Our findings suggest that the underlying physical meaning of the parameter c may be the time of the main shock in advance of the timing of the singularity point for an ideal response.

From Eqn. (24), it can be deduced that

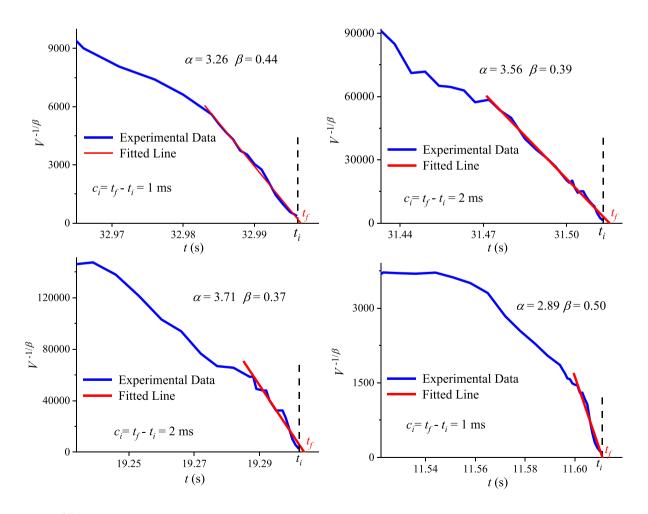$$V^{-1/\beta} = B^{-1/\beta} \ \left(c_i + t_i - t \right) \tag{26}$$

thus, $V^{-1/\beta}$ is linear in time. The linear trend of $V^{-1/\beta}$ with time for

Fig. 6. Defining slip instability transition point. Dash line denote instability transition time, t_i, defined by minimum value of ratio of slip velocity and acceleration and critical slip instability condition. It is shown that these two methods present consistent results determining the slip instability transition point. Straight yellow lines in above figures are fitted lines to linear relation of Eqn. (20), and t_f denotes the time of the predicted singularity in acceleration.

stick slip events, as shown in Fig. 7, confirms again that the power law representation of the precursory acceleration performs well as a predictor to the real onset of stick slip events. c_i defines the difference between the real t_i and projected t_f onset of stick slip and in current

experiments is very small - of the order of $c_i \sim 3$ ms. In particular, this difference is small in comparison to the advance warning, of the order of ~ 40–80 ms (Figs. 6 & 7), given of this onset – making the linearized relation a potentially robust and useful precursor.

Fig. 7. Curves of $V^{-1/\beta}$ versus time confirming the precursory power law acceleration and evaluating time difference between the true slip instability transition point t_i and that projected from where the linearized approximation becomes singular t_f. Red line: linear fitted line, and the intersection point t_f of this linearized extrapolation with the time axis is the projected singularity point. Compared with the vertical dashed line denoting the true initiation time of the slip instability, t_i.

These findings, including precursory power law behavior (Eqn. (21)), definition of dynamic instability (Eqn. (10)) with velocity and inertial effects and consistent predictions of three methods, are validated by experimental results when the normal stress is higher, e.g. normal stress is 6.8 MPa (Fig. 8).

5. Discussion

5.1. Transition to rupture

Brittle rupture may be analyzed in terms of a singularity in response to a finite increment of a driving variable (Salamon, 1970; Hudson et al., 1972; Hao et al., 2013; 2016; Xue et al., 2018; Wang et al. 2020). Typically, instability occurs at a singular point where an infinitesimal increment of the controlling variable induces a finite increment in response. Such perturbation analysis concludes that the tangent to the slope of the force versus displacement curve for a specimen must be equal to the negative stiffness of loading system (Salamon, 1970; Hudson et al., 1972; Hao et al., 2013; 2016; Xue et al., 2018; Wang et al. 2020).

Our results demonstrate that a limiting response velocity results in that the instability occurs in advance of the singular response. This instability transition leads to an increase in acceleration of the sliding after the instability transition that presents a distinctly different pattern to the precursory trend approaching it.

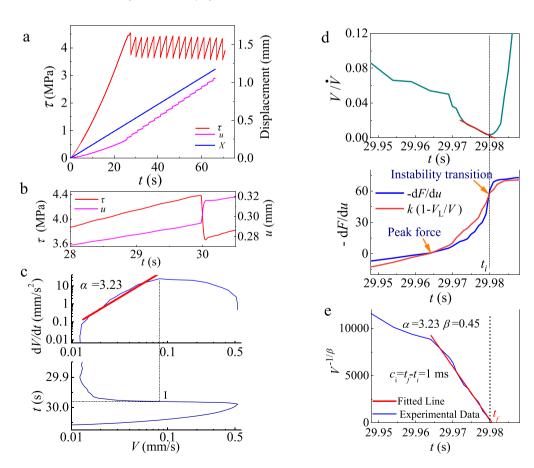### 5.2. Velocity and inertial effects on slip instability

Our findings indicate that load velocity and $m \, \mathrm{d}\dot{V}/\mathrm{d}f$ all exert significant influence on the form of the sliding velocity and the transition to slip instability. Dynamic influences on the slip instability transition may be represented by two dimensionless parameters – defined in this work as representing velocity ζ and an inertial χ effects.
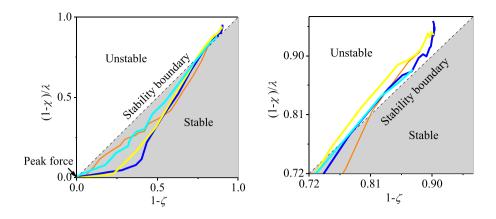
In the foregoing we do not recourse to rate and state friction, instead, basing the analysis on considerations of general energy balance. Our results decouple the separate effects of inertia and velocity on the transition to unstable slip. Our findings confirm that inertial effects impacting unstable slip are related to mass m and the ratio $\mathrm{d}\dot{V}/\mathrm{d}f$.

From accelerations and the known mass of the central sliding block, the instantaneous frictional resistance may be recovered from force balance as $f = F - m \, \dot{V}$. f is the sum of frictional resistance on the parallel laboratory faults of the double-direct shear sample. In our experiments, both the mass ($m \sim 0.3$ kg) of the sliding block and accelerations are small - so that the inertial force can be neglected. During individual stick slip events, the value of $\mathrm{d}\dot{V}/\mathrm{d}f$ is ~ 1.4 mm·s^2/N (Fig. 3f) at the slip instability transition point. As a consequence, the magnitude of the inertial coefficient χ is very small (of the order of 10^{-4}). The sliding velocity V is ~ 0.07 mm/s at the slip instability point (Fig. 4b and 5) and the load velocity V_L is 1 mm/min - thus the critical value of the velocity coefficient ζ is ~ 0.24. Therefore, in comparing the competing influences of velocity and inertia, that of velocity, embodied in ζ, is the more influential. Inertial effects (indexed by the coefficient χ) are important only when mass and change in acceleration become large.

Fig. 9 shows the variation of $(1-\zeta)$ versus $[(1-\chi)/\lambda]$ to illustrate the stable and unstable regimes in the current experiments defined by velocity and inertial effect coefficients of ζ and χ and where λ is the equivalent stiffness ratio shown in Eqn. (12). When $(1-\zeta)$ is equal to $[(1-\chi)/\lambda]$, this defines the critical boundary between stable and unstable slip

Fig. 8. Experimental results when the normal stress is 6.8 MPa. (a) Shear stress, τ, and sliding displacement, u. (b) Zoom-in on a single stick slip event. (c) One stick–slip event selected as an example to illustrate Voight's relation (red line) in fitting accelerations in the proximity of the slip instability transition I (upper) and the corresponding curve of velocity versus time (lower). (d),(e) Defining slip instability transition point through three methods.

Fig. 9. Experimental curves of $(1-\zeta)$ versus $[(1-\chi)/\lambda]$ showing unstable and stable regimes. Four representative experimental curves are shown (see Fig. 6) as examples, illustrating the transition from the point of peak force to the point where $[(1-\chi)/\lambda]$ reaches its maximum as a result fo the post-peak instability. The right sub-plot is an enlargement of that to the left, to zoom-in on the transition from stable to unstable regimes. Shaded area defines the stable regime and the dashed line the boundary in the transition from stable to unstable slip.

regimes, with the stability regime defined as the regime where $(1-\zeta) > [(1-\chi)/\lambda]$. At the point of peak force, both $(1-\zeta)$ and $[(1-\chi)/\lambda]$ are equal to zero. Then, both values of $(1-\zeta)$ and $[(1-\chi)/\lambda]$ in the current experiments increase in the stable regime until the trajectory of the response surface transits into the unstable regime. This is consistent with the theoretical instability condition defined in Eqn. (11). Conversely, sliding must remain stable if the trajectory is limited to below this boundary line.

5.3. Accelerating trend of precursory power law

Voight's relation (Voight, 1988; 1989) describes an acceleration in response quantities (displacements, AE) as a system approaches a singular/catastrophic point. For stick-slip instabilities the form of this acceleration divides across an instability transition point – these represent a precursory constant acceleration followed by an unstable accelerating phase of sliding.

This bifurcation in response occurs as the system evolves from stable sliding before the instability transition to accelerating sliding (Fig. 4b and 5) after it. We have demonstrated that a power law definition of acceleration (Eqns. (20) and (26)) represents the characteristics of the system as it approaches the instability transition point.

5.4. Implication for earthquake mechanics

As applied to earthquake mechanics, these current experimental results illustrate, in detail, the various processes of sliding from static, evolving to the onset of acceleration, unstable slip, deceleration and finally back to the static state. Our findings highlight five typical stages involved in stick-slip cycles defined by evolutions in velocity, acceleration, frictional and shear forces. These are, incrementally: 1) monotonic increases in sliding acceleration; 2) decrease in acceleration; 3) deceleration; 4) "undershoot" occurring until a minimum shear force results that represents the end of the unstable slip cycle; 5) intermediate adjustment stage or a return from acceleration "undershoot" to the quasi-static state. Distinguishing these processes of fault sliding is a foundational in understanding the earthquake cycle and its arrest.

Our experiments give direct measurements of sliding through the direct measurement of displacement of the slider. Experimental results charting the evolution of the frictional strength and sliding yield fundamental constraints on the description of constitutive laws representing fault sliding and its contribution to earthquake mechanics.

Defining instability of faults and identifying reliable precursors (Geller, 1997; Bowman et al., 1998) based on the rational evaluation of monitored quantities is central in building a reliable model of earthquake processes. Our findings define a criterion separating stable and unstable regimes of sliding behaviours through the velocity and inertial effect coefficient phases. This criterion is cross-validated against precursory power law accelerating slip in our experiments through the monitoring of deformation and force evolution. This yields insights in understanding the instbliliy transition of faults and suggests a way to explore mechanisms of natural earthquakes by monitoring such measurable signals.

6. Conclusions

The prior analysis indicates that both velocity and inertia impact the timing of the slip instability transition relative to that predicted from a static analysis. These velocity ζ and inertial χ effects impact critical stiffness defining the slip instability transition by respectively increasing or decreasing critical stiffness. The velocity effect coefficient ζ represents the ratio of sliding velocity to load velocity and the inertial effect depends on mass and the relative change in acceleration with respect to frictional resistance. The inertial effect becomes important only when mass or the change in acceleration are very large, resulting in χ being of the order of unity. In the current experiments, ζ is ~ 0.24 and χ is of the order of 10^{-4}.

The entire unstable sliding process transits successively through acceleration to deceleration with characteristic features on this repetitive stick-slip path of instability successively representing maximum acceleration, then maximum velocity followed by a minimum acceleration to a minimum force point - with this then followed by a return to stable sliding to reset behavior ready for the initiation of the next cycle.

The evolving trend of sliding velocity in the proximity of the slip instability transition point is accurately described by Voight's relation and follows a power law relationship of the form $V = B \ (c_i + t_i - t)^{-\beta}$. c_i represents the time difference between the dynamic slip instability transition point t_i and the ideal singularity point. The power law exponent β in experiments presented here is ~ 0.42 with the exponent of $\alpha \sim 3.4$. This power law behavior clearly distinguishes the precursory acceleration from the subsequent unstable accelerating process.

Three independent methods are used to define the stability transition, including (i) linear $V/\dot{V} = (\alpha - 1) \ (t_f - t)$, (ii) criticality conditions $- \ \mathrm{d}F/\mathrm{d}u = k \ (1 - V_L/V)$ and (iii) power law $V = B \ (c_i + t_i - t)^{-\beta}$. All three methods provide consistent and confirmatory results in determining the timing of the slip instability transition, as confirmed by the stick slip data. The error between the projected time of onset of stick slip and the real timing is small in comparison to the lead time afforded by the fitting of the velocity data, suggesting that this characterization may be used to forewarn of the onset – as a precursory signal with potentially sufficient time to mitigate impacts.

Declaration of Competing Interest

The authors declare that they have no known competing financial interests or personal relationships that could have appeared to influence the work reported in this paper.

Data availability

Data will be made available on request.

Acknowledgments

References

Baumberger, T., Heslot, F., Perrin, B., 1994. Crossover from creep to inertial motion in friction dynamics. Nature 367 (6463), 544–546.

Bell, A.F., Naylor, M., Heap, M.J., Main, I.G., 2011. Forecasting volcanic eruptions and other material failure phenomena: an evaluation of the failure forecast method. Geophys. Res. Lett. 38 (15), L15304.

Bhushan, B., 2013. Introduction to tribology, 2nd Edition. Publication), John Wiley & Sons Ltd.

Bowman, D., Ouillon, G., Sammis, C.G., Sornette, A., Sornette, D., 1998. An Observational Test of the Critical Earthquake Concept. J. Geophys. Res. 103 (B10), 24359–24372.

Brace, W.F., Byerlee, J.D., 1966. Stick–slip as a mechanism for earthquakes. Science 153 (3739), 990–992.

Carlson, J.M., Batista, A.A., 1996. Constitutive relation for the friction between lubricated surfaces. Phys. Rev. E 53 (4), 4153–4165.

Cui, D., Wu, W., Xiang, W., Doanh, T., Chen, Q., Wang, S., Liu, Q., Wang, J., 2017. Stick-slip behaviours of dry glass beads in triaxial compression. Granular Matter 19 (1). https://doi.org/10.1007/s10035-016-0682-5.

Dieterich, J.H., 1979. Modeling of rock friction: 1. experimental results and constitutive equations. J. Geophys. Res. 84, 2161–2168.

Fávero Neto, A.H., Askarinejad, A., Springman, S.M., Borja, R.I., 2020. Simulation of debris flow on an instrumented test slope using an updated Lagrangian continuum particle method. Acta Geotech. 15 (10), 2757–2777.

Geller, R.S., 1997. Earthquak prediction: a critical review. Geophys. J. Int 131, 425–450.

Gnecco, E., Hennig, J., Moayedi, E., Wondraczek, L., 2018. Surface rippling of silica glass surfaces scraped by a diamond indenter. Phys. Rev. Mat. 2, 115601.

Gu, J.-C., Rice, J.R., Ruina, A.L., Tse, S.T., 1984. Slip motion and stability of a single degree of freedom elastic system with rate and state dependent friction. J. Mech. Phys. Solids 32 (3), 167–196.

Gu, Y., Wong, T.-F., 1991. Effects of loading velocity, stiffness, and inertia on the dynamics of a single degree of freedom spring-slider system. J. Geophys. Res. 96 (B13), 21677–21691.

Hainzl, S., Zoller, G., Kurths, J., 1999. Similar power laws for foreshock and aftershock sequences in a spring-block model for earthquakes. J. Geophys. Res. 104 (B4), 7243–7253.

Hao, S.W., Rong, F., Lu, M.F., Wang, H.Y., Xia, M.F., Ke, F.J., Bai, Y.L., 2013. Power-law singularity as a possible catastrophe warning observed in rock experiments. Int. J. Rock Mech. Min. Sci. 60, 253–262.

Hao, S.W., Liu, C., Lu, C.S., Elsworth, D., 2016. A relation to predict the failure of materials and potential application to volcanic eruptions and landslides. Sci. Rep. 6, 27877.

Hao, S.W., Yang, H., Elsworth, D., 2017. An accelerating precursor to predict "time-to-failure" in creep and volcanic eruptions. J. Volcanol. Geotherm. Res. 343, 252–262.

Hudson, J.A., Crouch, S.L., Fairhurst, C., 1972. Soft, stiff and servo-controlled testing machines: A review with reference to rock failure. Eng. Geol. 6 (3), 155–189.

Im, K., Elsworth, D., Marone, C., Leeman, J., 2017. The impact of frictional healing on stick–slip recurrence interval and stress drop: implications for earthquake scaling. J. Geophys. Res. 122, 10102–10117.

Im, K., Marone, C., Elsworth, D., 2019. The transition from steady frictional sliding to inertia-dominated instability with rate and state friction. J. Mech. Phys. Solids 122, 116–125.

Jones, L.M., Molnar, P., 1979. Some characteristics of foreshocks and their possible relationship to earthquake prediction and premonitory slip on faults. J. Geophys. Res. 84 (B7), 3596–3608.

Kasyap, S.S., Senetakis, K., Coop, M.R. et al., 2021. Micromechanical behaviour in shearing of reproduced flat LBS grains with strong and weak artificial bonds. Acta Geotech. 16, 1355-1376 (2021).

Kilburn, C.R.J., 2003. Multiscale fracturing as a key to forecasting volcanic eruptions. J. Volcanol. Geotherm. Res. 125 (3-4), 271–289.

Kilburn, C., 2012. Precursory deformation and fracture before brittle rock failure and potential application to volcanic unrest. J. Geophys. Res. 117 (B2), n/a–n/a.

Kilburn, C.R.J., Voight, B., 1998. Slow rock fracture as eruption precursor at Soufriere Hills, volcano. Montserrat. Geophys. Res. Lett. 25 (19), 3665–3668.

Lin, W., Liu, A., Mao, W., Koseki, J., 2020. Acoustic emission characteristics of a dry sandy soil subjected to drained triaxial compression. Acta Geotech. 15 (9), 2493–2506.

Main, I.G., 1999. Applicability of time-to-failure analysis to accelerated strain before earthquakes and volcanic eruptions. Geophys. J. Int. 139 (3), F1–F6.

Rabinowicz, E., 1956. Stick and slip. Sci. Am. 194 (5), 109–119.

Rice, J.R., Ruina, A.L., 1983. Stability of steady frictional slipping. J. Appl. Mech. 50 (2), 343–349.

Rice, J.R., Tse, S.T., 1986. Dynamic motion of a single degree of freedom system following a rate and state dependent friction law. J. Geophys. Res. 91 (1), 521–530.

Ruina, A., 1983. Slip instability and state variable friction laws. J. Geophys. Res. 88 (B12), 10359–10370.

Salamon, M.D.G., 1970. Stability, instability and design of pillar workings. Int. J. Rock Mech. Min. Sci. 7 (6), 613–631.

Scholz, C.H., 1998. Earthquakes and friction laws. Nature 391 (6662), 37–42.

Shimamoto, T., Handin, J., Logan, J.M., 1980. Specimen-apparatus interaction during stick–slip in a triaxial compression machine: a decoupled two-degree- of-freedom model. Tectonophysics 67 (3-4), 175–205.

Urbakh, M., Klafter, J., Gourdon, D., Israelachvili, J., 2004. The nonlinear nature of friction. Nature 430 (6999), 525–528.

Utsu, T., Ogata, Y., S, R., Matsu'ura, 1995. The centenary of the Omori Formula for a decay law of aftershock activity. J. Phys. Earth 43 (1), 1–33.

Voight, B., 1988. A method for prediction of volcanic eruptions. Nature 332 (6160), 125–130.

Voight, B., 1989. A relation to describe rate-dependent material failure. Science 243 (4888), 200–203.

Voight, B., Cornelius, R.R., 1991. Prospects for eruption prediction in near real-time. Nature 350 (6320), 695–698.

Wang, H., Hao, S.W., Elsworth, D., 2020. Non-monotonic precursory signals to multi-scale catastrophic failures. Int. J. Fract. 226 (2), 233–242.

Xing, H., Han, Z., 2020. Caving-induced fault reactivation behavior and its effects on mining safety with a multiple seam context. Acta Geotech. 15, 3461–3481.

Xue, J., Hao, S., Wang, J., Ke, F., Lu, C., Bai, Y., 2018. The changeable power-law singularity and its application to prediction of catastrophic rupture in uniaxial compressive tests of geo-media. J. Geophys. Res. Solid Earth 123 (4), 2645–2657.